Hydrazide- and Diazole-Linked Covalent Organic Frameworks and Their Water Harvesting Properties

Ha L. Nguyen,[†,‡,◊] Cornelius Gropp,[†,◊] Anna Möckel,[†] Nikita Hanikel,[†] Alicia Lund,[∇] and Omar M. Yaghi[*,†,‡]

[†]Department of Chemistry, University of California–Berkeley; Kavli Energy Nanoscience Institute at UC Berkeley; and Berkeley Global Science Institute, Berkeley, California 94720, United States

[‡]Joint UAEU–UC Berkeley Laboratories for Materials Innovations, United Arab Emirates University, Al-Ain 15551, United Arab Emirates

[∇]Department of Chemistry, University of California–Berkeley, Berkeley, California 94720, United States

ABSTRACT: We report a retrosynthetic strategy and its implementation to making covalent organic frameworks (COFs) with irreversible hydrazide and diazole (oxadiazole and thiadiozole) linkages. This involved the synthesis of a series of 2D and 3D hydrazine-linked frameworks, followed by their oxidation and dehydrative cyclization. Each linkage synthesis and functional group transformation—hydrazine, hydrazide, oxadiazole, and thiadiazole—was evidenced by ^{15}N multi-CP-MAS NMR. In addition, the isothermal water uptake profiles of these frameworks were studied, leading to the discovery that one hydrazide-linked COF is suitable for water harvesting from air in arid conditions. These COFs displayed characteristic S-shaped water sorption profiles, a steep pore-filling step below 18% relative humidity at 25 °C, and a total uptake capacity of 0.45 g g^{-1} at P/P_{sat} = 0.95. In addition, a total of ten 2D and 3D structures with various such linkages were studies for their affinity to water. We found that even small changes made on the molecular level can lead to major differences in the water isotherm profiles and therefore pointing to the utility of water sorption analysis as a complementary analytical tool to study linkage transformations.

INTRODUCTION

Many multi-step organic synthetic methods have been successfully translated to the solid state.[1–4] This practice has become especially attractive for the synthesis of new covalent organic frameworks (COFs).[5–8] Their hallmark features, porosity and crystallinity, allow chemical transformations to be done on the framework and enable rigorous analysis of concurrent structural changes through diffraction and spectroscopic techniques.[5,6]

The synthesis of COFs relies on an initial reversible step to guide the covalent assembly of organic building units into extended and crystalline structures.[9–12] This step can be followed by one or more postsynthetic transformations, leading to structural complexity and function of the framework.[5,8,10,11] This has been demonstrated for a number of imine-linked COFs, but synthetically more challenging moieties, such as heterocycles, are still rare.[13–15]

Here, we developed diazole-linked COFs following a retrosynthetic approach. This provided us with the synthetic challenge to explore disconnection sequences leading to an initial reversible assembly of the framework from organic building units as illustrated in Scheme 1 for transformation of irreversible diazoles to irreversible hydrazides to reversible hydrazines. We were able to study the impact of each molecular transformation on the properties of the framework. Considering the hydrophilic nature of the proposed diazole linkages, we chose to study the water uptake after each synthetic transformation.[16,17] This not only allowed us to explore new sorbents for water harvesting from air, but also provided us with additional insight into the micro- and macroscopic changes occurring on the framework.

Scheme 1. Synthetic strategy for diazole-linked COFs. This strategy was applied to a molecular model system and two 2D (**hcb**, **sql**) and one 3D (**dia**) COFs.
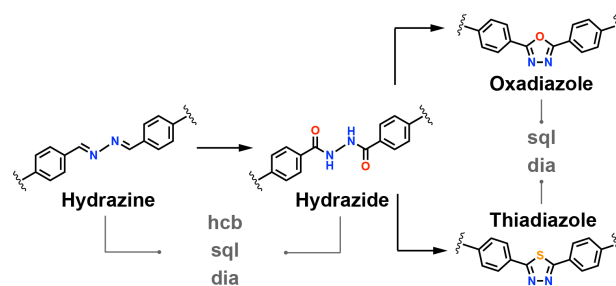
Our synthetic strategy towards oxa- and thiadiazole-linked COFs is based on the reversible formation of hydrazine-linked COFs, followed by postsynthetic oxidation to the hydrazide-linkage and cyclization to afford the heterocycles (Scheme 1). We first demonstrated the feasibility of this route on a molecular model system. Then, we explored its transferability to the solid-state by synthesizing two 2D COFs with honeycomb (**hcb**) and square-lattice (**sql**) topologies and one 3D COF with diamond (**dia**) topology. In total, ten COFs were synthesized, 8 of which are new COFs with hydrazine, hydrazide, and diazole linkages; the latter two are new linkages in COF chemistry. The COFs were analyzed by ^{15}N multiple cross-polarization magic-angle spinning spectroscopy (multi-CP-MAS NMR),[18] giving a quantitative readout of the chemical transformations. Fourier-transform infrared (FT-IR), solid- and solution-state nuclear magnetic resonance (NMR) spectroscopies, elemental analysis (EA), thermogravimetric analysis (TGA), powder X-ray diffraction (PXRD), and nitrogen sorption substantiated the structural and compositional integrity of the frameworks.

RESULTS AND DISCUSSION

To show the viability of our retrosynthetic strategy, we first synthesized a hydrazine molecular model compound, 1,2-benzylidenehydrazine, from benzaldehyde and hydrazine with quantitative yield (Scheme 1).[19] The hydrazine compound was subsequently oxidized to afford the hydrazide molecular model using previously reported conditions for the conversion of imines to amides in COFs.[5] The oxadiazole and thiadiazole compounds were then synthesized from the hydrazide through dehydrative cyclization using $POCl_3$ and P_2S_5, respectively.[20,21] The cyclization step occurred with high yields (>90%), further indicating applicability of the three-step synthetic route to the synthesis of extended structures. All compounds were fully characterized and served as structural models to their solid-state analogues (see Supporting Information, SI, Section S2).

The transferability of the three-step synthesis to the solid state was successfully demonstrated through the synthesis of two 2D and one 3D hydrazine-linked COFs (Scheme 2). AB-COF[22,23] was produced from the trigonal-planar 1,3,5-benzenetrialdehyde (BTA) and linear hydrazine (Hy), and crystallized in the **hcb** topology with the reticular formula [(BTA)$_2$(Hy)$_3$]$_{hydrazine}$. Py-COF-2D[24] is comprised of the square-planar 1,3,6,8-tetrakis(p-formylphenyl)pyrene (TFPPy) unit and Hy and crystallized in the **sql** topology with the reticular formula [(TFPPy)(Hy)$_2$]$_{hydrazine}$. Lastly, COF-670-hydrazine was synthesized from the tetrahedral 4,4',4'',4'''-methanetetrayltetrabenzaldehyde (MTBA) and Hy and crystallized in the **dia** topology with the reticular formula [(MTBA)(Hy)$_2$]$_{hydrazine}$ (Scheme 2). While AB-COF and Py-COF-2D have been previously reported,[22,23] a hydrazine-linked 3D COF, COF-670-hydrazine, has not been reported to date.

We first explored the oxidation of the hydrazine-linked AB-COF by subjecting it to our reported oxidation conditions[5] involving the use of $NaClO_2$ as oxidant in aqueous acidic medium in the presence of 2-methyl-2-butene over three days to obtain COF-480-hydrazide (see SI, Section S2). FT-IR spectroscopic traces of the product indicated attenuation of the imine band at 1625 cm^{-1} corresponding to the hydrazine linkages and an emerging band at 1674 cm^{-1}, which was assigned to the carbonyl stretching vibration of the hydrazide moiety (see SI, Section S3). The solid-state ^{15}N multi-CP-MAS NMR spectroscopy[18] was performed on a 50% ^{15}N-labeled sample and revealed the partial conversion of the hydrazine to the hydrazide (see SI, Section S4). Here, the resonances corresponding to the functionalities were fit to Gaussian line shapes and their relative areas were compared. This analysis correlated well with the atomic composition determined by EA (see SI, Section S2). TGA under nitrogen and air flow revealed an onset in decomposition for the pristine and the oxidized samples at around 380 °C.
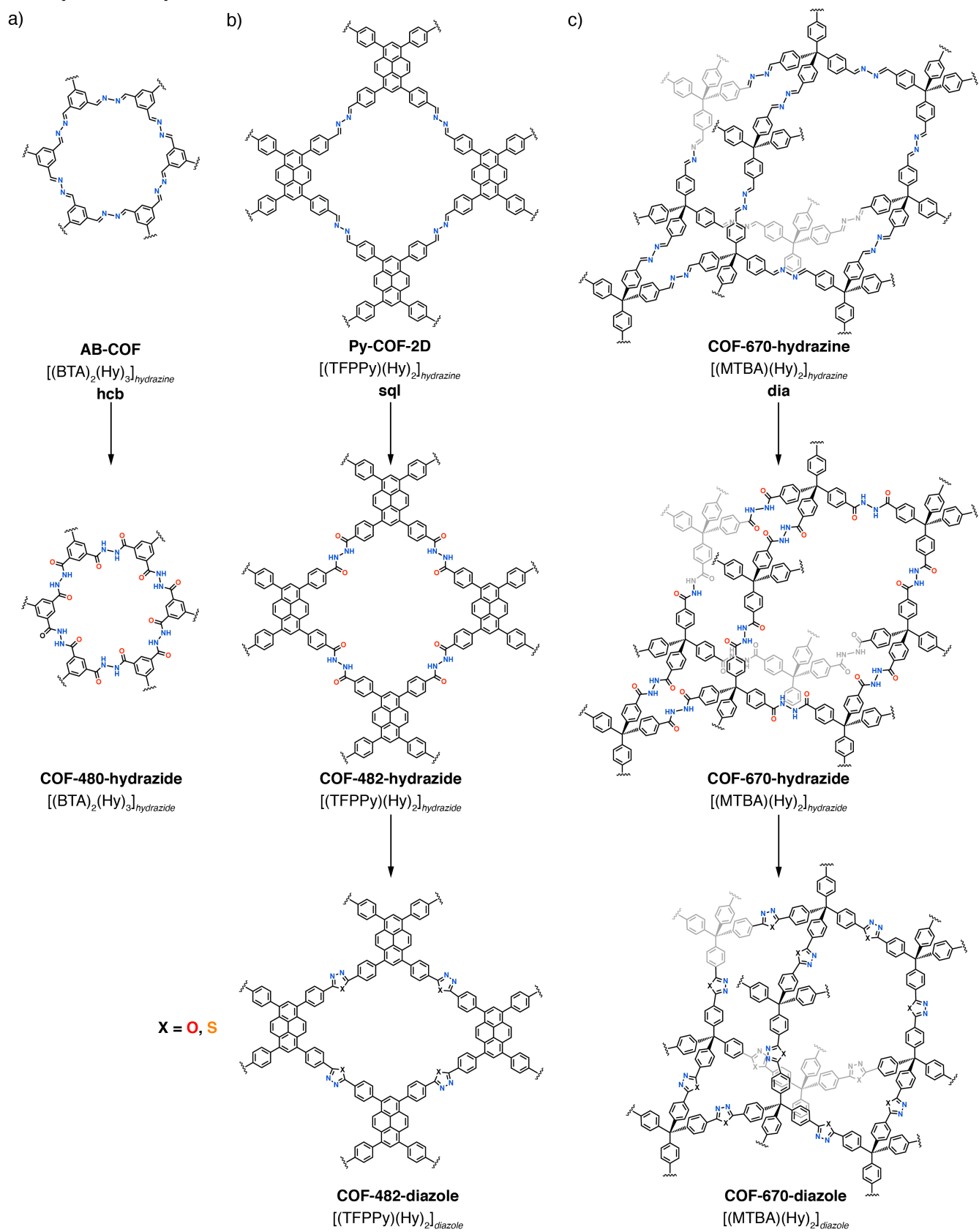
PXRD analysis of the microcrystalline powder confirmed retention of crystallinity after oxidation and did not reveal additional diffraction peaks associated with hydrolyzed starting materials or additives (see SI, Section S6). The PXRD pattern of AB-COF shows high-intensity peaks at 6.8°, 11.8°, and 26.4° 2θ values, associated with the (100), (1-20), and (002) lattice planes. After oxidation, the broad peak indexed as the lattice plane (002) shifts to a higher 2θ value (26.6° 2θ), resulting from changes in the interlayer stacking of the structure.

N_2 sorption analysis at 77 K of the pristine AB-COF and COF-480-hydrazide demonstrated permanent porosity and revealed a Type I isotherm, indicating a micropore structure. The Brunauer–Emmett–Teller (BET) surface areas were calculated to be 1209 m^2 g^{-1} and 989 m^2 g^{-1}, respectively. The pore size distribution, estimated from the N_2 isotherms and calculated by density functional theory (DFT) using the cylinder geometry, indicated comparable pore sizes of around 11 Å in diameter (see SI, Section S7).

To gain further insight into the impact of the chemical transformations on the water sorption behavior, we measured the water sorption isotherms at 15 °C, 25 °C, and 35 °C (Figure 1a, b). AB-COF displays an S-shaped water sorption isotherm with a steep pore-filling step at around 23% relative humidity (RH) at 25 °C (Figure 1a). The maximal uptake at $P/P_{sat} = 0.95$ reaches a total uptake capacity of 0.45 g g^{-1}. After oxidation, the water sorption isotherm of COF-480-hydrazide substantially shifts to lower RH with a steep pore-filling step at 18%—thus extending the RH range at which COF-480-hydrazide can operate to more arid conditions. Importantly, the COF preserves its total water uptake uptake capacity of around 0.45 g g^{-1} at $P/P_{sat} = 0.95$ (25 °C).

Furthermore, the water sorption isotherm profiles are retained at 15 °C and 35 °C, indicating robust sorption behavior under varying temperatures. The increased water uptake capacity at lower RH upon oxidation indicated stronger water–framework interactions during the pore-

Scheme 2. Overview of the synthesis of (a) 2D **hcb**, (b) 2D **sql**, and (c) 3D **dia** hydrazide-, and diazole-linked COFs. The synthesis of hydrazine-linked COFs is detailed in the SI.

a)

b)

c)

AB-COF
[(BTA)$_2$(Hy)$_3$]$_{hydrazine}$
hcb

Py-COF-2D
[(TFPPy)(Hy)$_2$]$_{hydrazine}$
sql

COF-670-hydrazine
[(MTBA)(Hy)$_2$]$_{hydrazine}$
dia

COF-480-hydrazide
[(BTA)$_2$(Hy)$_3$]$_{hydrazide}$

COF-482-hydrazide
[(TFPPy)(Hy)$_2$]$_{hydrazide}$

COF-670-hydrazide
[(MTBA)(Hy)$_2$]$_{hydrazide}$

X = O, S

COF-482-diazole
[(TFPPy)(Hy)$_2$]$_{diazole}$

COF-670-diazole
[(MTBA)(Hy)$_2$]$_{diazole}$

filling step.[25,26] To evaluate the strength of these interactions, the isosteric heat of water adsorption (Q_{st}) was calculated with the Clausius–Clapeyron equation using the water isotherms at 15 °C, 25 °C, and 35 °C. The Q_{st} was
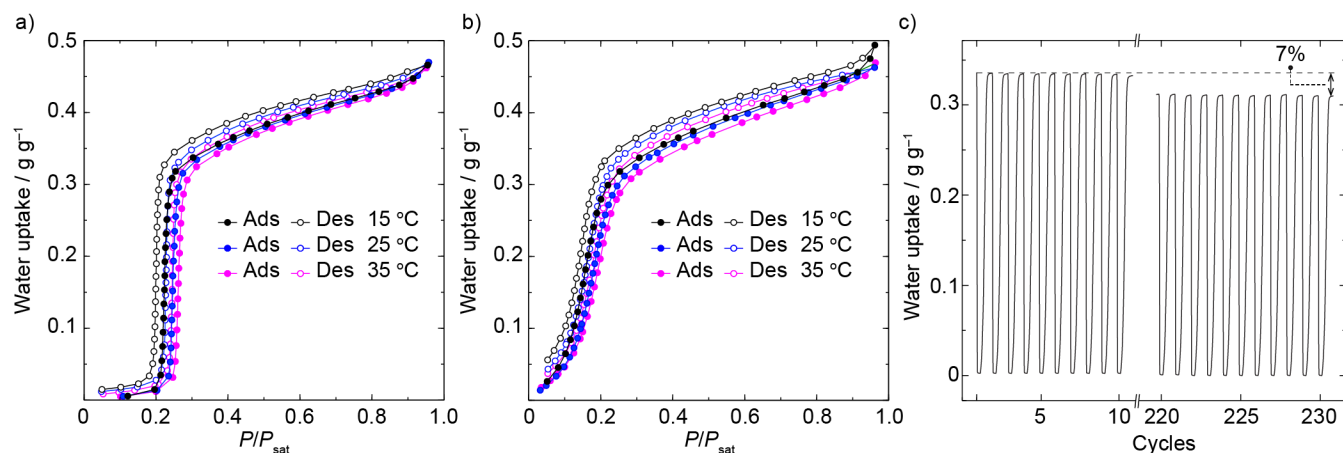
Figure 1. Water vapor sorption analysis of AB-COF (a) and COF-480-hydrazide (b) at different temperatures (15 °C, 25 °C, and 35 °C). P: water vapor pressure. P_{sat}: saturation water vapor pressure at the given temperature. Water cycling stability test of 230 adsorption–desorption cycles of COF-480-hydrazide (c) subjected to an isobaric (1.7 kPa water vapor) temperature-swing adsorption between 30°C and 85 °C, corresponding to 40% and 3% RH, respectively; Full dataset reported in the SI, Section S8.

estimated to be 49 kJ mol^{-1} for the pristine AB-COF and 50.5 kJ mol^{-1} for the oxidized COF-480-hydrazide. A ΔQ_{st}= 1.5 kJ mol^{-1} upon oxidation likely results from the stronger hydrogen-bonding donor and acceptor sites in the framework, given that both COFs show comparable pore diameters of around 11 Å.

It is noteworthy that even the partial conversion significantly shifted the water uptake to lower RH and resulted in an increase of water affinity to the framework. Thus, COF-480-hydrazide extracts water from air at even lower humidity compared to the pristine hydrazine-linked COF, AB-COF.[23]

To test the long-term stability of COF-480-hydrazide over multiple water adsorption–desorption cycles, we subjected the COF to an isobaric (1.7 kPa water vapor) temperature-swing adsorption between 30°C and 85 °C, corresponding to 40% and 3% RH, respectively. The water uptake working capacity under these conditions was 0.33 g g^{-1}. After 230 adsorption–desorption cycles, we observed a reduction of the working capacity by 7% (Figure 1c). This is attributed to partial hydrolysis of the sample upon long-term exposure to water vapor at elevated temperature.

Next, we pursued the oxidation of the hydrazine-linked Py-COF-2D to COF-482-hydrazide followed by dehydrative cyclization. For the oxidation we applied the same oxidation conditions as described for the AB-COF. Similarly, we observed attenuation of the characteristic imine band at 1625 cm^{-1} in the FT-IR spectroscopic traces and appearance of the carbonyl band at 1674 cm^{-1}. The solid-state ^{15}N multi-CP-MAS NMR spectroscopy on a 50% ^{15}N-labeled sample indicated a partial conversion of the hydrazine- to the hydrazide-linkage (see SI, Section S4). We then subjected COF-482-hydrazide to POCl$_3$ (neat) at 100 °C and P$_2$S$_5$ (7 equiv.) at 110 °C for 24 h to obtain COF-482-oxadiazole and COF-482-thiadiazole, respectively (see SI, Section S2).

After washing, solvent-exchange, and activation of the samples, the FT-IR spectra displayed characteristic bands associated with the oxadiazole and thiadiazole moieties. Additionally, we confirmed the conversion through quantitative solid-state ^{15}N CP-MAS NMR spectroscopy, where we observed a shift of the hydrazide ^{15}N peak at 171.3 ppm to the thiadiazole ^{15}N peak at 173.3 ppm (see SI, Section S5). We recognize the ambiguity of assigning the ^{15}N peak of thiadiazole-linked COFs due to overlapping chemical shifts and incomplete conversion. TGA under nitrogen and air flow revealed a comparable onset in decomposition for the pristine, oxidized, and cyclized samples at around 500 °C.

PXRD analysis of the microcrystalline powder of Py-COF-2D, COF-482-hydrazide, COF-482-oxadiazole, and COF-482-thiadiazole COFs indicated retention of crystallinity over the three-step synthesis (see SI, section S6). Furthermore, the PXRD traces indicated a shift of the highest intensity peaks from 4.5° 2θ, associated with the (1-10) lattice plane, for the hydrazine-linked COF to 4.6° 2θ for the hydrazide and 4.7° 2θ for both diazole-linked COFs. This observation correlates well with the anticipated changes in unit cell parameters upon oxidation and cyclization as observed in the molecular models (see SI, Section S6).

N$_2$ sorption analysis at 77 K of all four samples demonstrated permanent porosity and revealed a Type I isotherm, indicating a micropore structure. The calculated BET surface areas amounted to 1850 m^2 g^{-1} for the hydrazine-linked Py-COF-2D and 1700 m^2 g^{-1} for COF-482-hydrazide. Upon cyclization the BET surface area was decreased to 1411 m^2 g^{-1} and 1363 m^2 g^{-1} for COF-482-oxadiazole and COF-482-thiadiazole, respectively. The reduction in surface area is in line with the weight increase upon oxidation and cyclization. The pore size distribution, calculated from the N2 adsorption isotherms using the above-described parameters, indicated two kinds of pores with diameters of 15.9 Å and 18.5 Å for Py-COF-2D and 15.4 Å and 18.5 Å for

the oxidized COF-482-hydrazide. The pore diameters slightly changed upon cyclization to 15.5 Å and 18.4 Å for both COF-482-oxadiazole and COF-482-thiadiazole.

The pristine Py-COF-2D displayed an S-shaped water sorption isotherm with a steep pore-filling step at around 52% RH and a total uptake 0.75 g g^{-1} at 25 °C (Figure 2). Upon oxidation, the isotherm profile significantly shifted to 42% RH with a slightly lower total uptake of 0.70 g g^{-1} at 25 °C. The shift of the pore-filling step to lower RH upon oxidation is in line with our previous observation in AB-COF and presumably stems from the incorporation of the more polar hydrazide functionalities into the framework. Interestingly, we observed a shift back to higher RH upon cyclization to the oxadiazoles and thiadiazoles with the pore-filling step at around 52% RH and total uptake values of 0.50 g g^{-1} and 0.60 g g^{-1} at 25 °C (Figure 2), respectively.
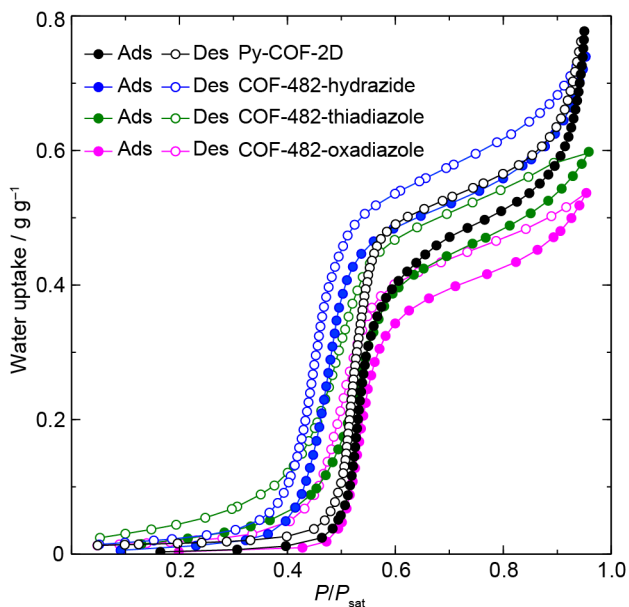

Figure 2. Overlay of water isotherms of Py-COF-2D, COF-482-hydrazide, COF-482-thiadiazole, and COF-482-oxadiazole at 25 °C. P: water vapor pressure. P_{sat}: saturation water vapor pressure.

This is one of the first examples where postsynthetic transformations on COFs enabled a shift of the pore-filling step of the water isotherms to lower or higher RH.[27,28] The difference in the Q_{st} between the pristine Py-COF-2D and COF-482-hydrazide, calculated from the water sorption isotherms at 15 °C, 25 °C, and 35 °C, amounted to ΔQ_{st}= 2 kJ mol^{-1} (Q_{st}= 45 kJ mol^{-1} and 47 kJ mol^{-1}, respectively). A comparable ΔQ_{st} of the pristine sample and the oxidized hydrazide sample was also observed for AB-COF and COF-480-hydrazide.

Finally, to demonstrate our three-step synthesis of diazole-linked COFs in 3D, we first synthesized a hydrazine-linked COF-670-hydrazine from the tetrahedral MTBA and linear hydrazine building units (Scheme 1c and Figure 3a). The structure crystallized in the **dia** topology with 6-fold interpenetration (see SI, Section S6). Upon oxidation, we observed attenuation of the characteristic imine band at 1625 cm^{-1} in the FT-IR spectroscopic traces and appearance

of band at 1674 cm^{-1} (see SI, Section S3). The solid-state ^{15}N CP-MAS NMR spectroscopy on a 50% ^{15}N-labeled sample indicated a partial conversion of the hydrazine- to the hydrazide-linkage (Figure 3b and SI, Section S4).

Despite the low conversion of the hydrazine- to hydrazide-functionalities, we subjected the hydrazide-linked 3D COF to POCl$_3$ (neat) at 100 °C and P$_2$S$_5$ (4 equiv.) at 110 °C for 24 h to obtain COF-670-oxadiazole and COF-670-thiadiazole, respectively (Figure 3c and SI, Section S2). After washing, solvent-exchange, and activation of the sample, we measured the solid-state ^{15}N CP-MAS NMR spectroscopy. Here, we observed a shift of the ^{15}N hydrazide peak from 169.2 ppm to 170.8 ppm (see SI, Section S4). TGA under nitrogen and air flow revealed an increase in thermal stability upon oxidation and cyclization of the hydrazine-linked COF. Here, COF-670-hydrazine, COF-670-hydrazide, COF-670-oxadiazole, and COF-670-thiadiazole showed an onset in thermal decomposition at around 350 °C.

PXRD analysis of the microcrystalline powder of the hydrazine-linked COF and comparison with structural models of varying degrees of interpenetration allowed us to assign the degree of interpenetration to 6-fold (Figure 3d, e). After oxidation and cyclization, the PXRD indicated retention of the crystallinity (Figure 3f and SI section S6). Furthermore, the PXRD traces indicated a small shift of the highest intensity peaks at 9.4° 2θ, associated with the (020) lattice plane, for the hydrazine-linked COF to 9.5° 2θ for the hydrazide and 9.6° 2θ for both the diazole-linked COFs. This observation correlated well with the anticipated changes in unit cell parameters upon oxidation and cyclization as observed in the molecular models (see SI, Section S6). We also observed shifts to higher 2θ values for designated reflections occurring between 13° to 25°.

N$_2$ sorption analysis at 77 K of all four samples demonstrated permanent porosity and revealed a Type I isotherm, indicating a micropore structure. The calculated BET surface areas amounted to 1209 m^2 g^{-1} for the hydrazine-linked COF-670-hydrazine and 699 m^2 g^{-1} for COF-670-hydrazide. Upon cyclization the surface area amounted to 661 m^2 g^{-1} and 576 m^2 g^{-1} for COF-670-oxadiazole and COF-670-thiadiazole, respectively. The latter indicates negligible loss in surface area upon cyclization. The pore size distributions, calculated from the N$_2$ adsorption isotherms using the above-described parameters, indicated overall retention of the pore diameters of 6 Å after oxidation and cyclization (see SI, Section S7).

The pristine COF-670-hydrazine displayed a water sorption isotherm with a slightly sloped pore-filling step at around 43% RH and a total uptake of 0.33 g g^{-1} at 25 °C (see SI, Section S8). Oxidation and cyclization did not significantly influence the water isotherm profiles and is in line with the low conversion observed in the oxidation and cyclization steps (see SI, Section S8).
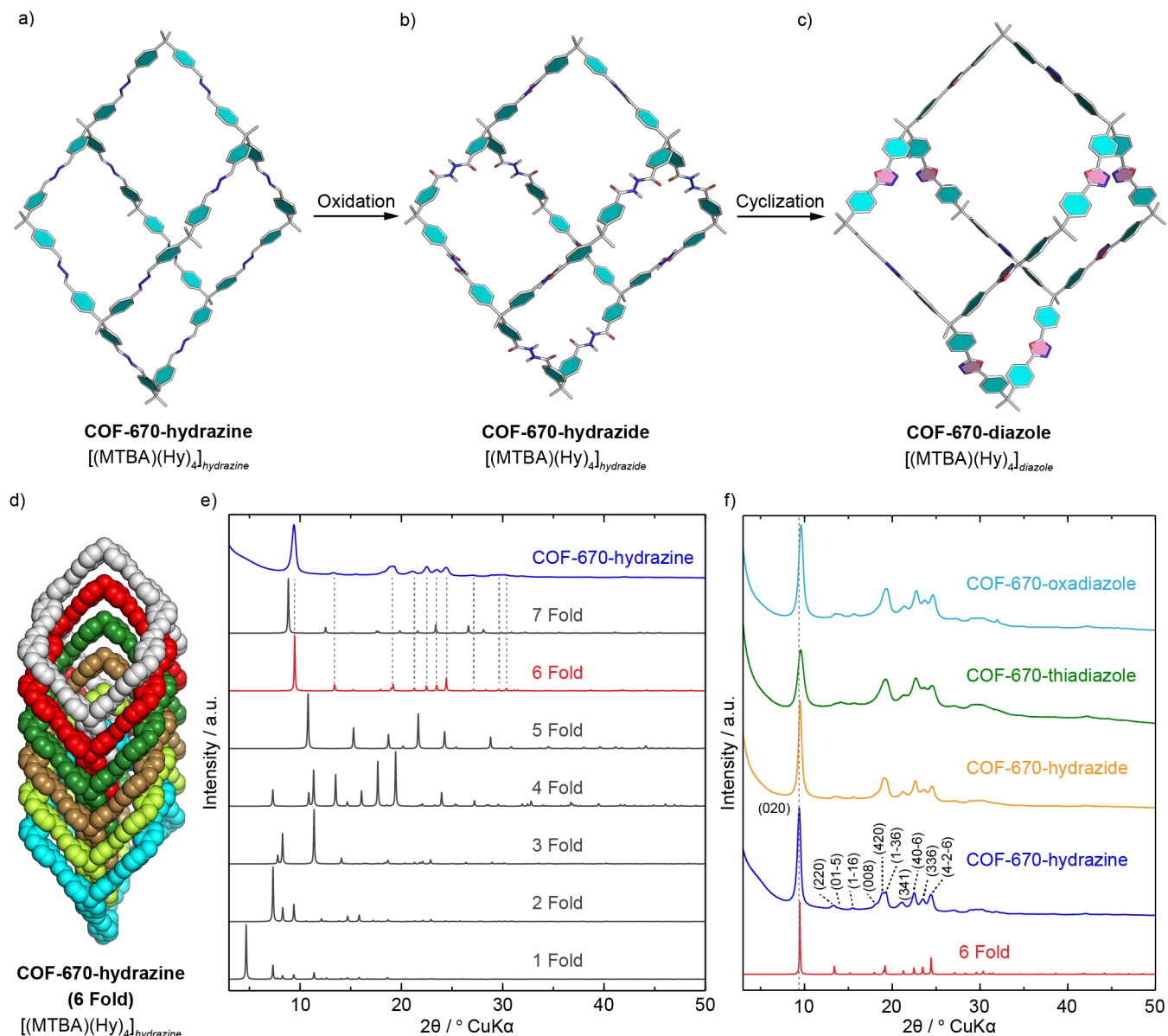
CONCLUSION

Figure 3. Structural models of the single framework of COF-670-hydrazine (a) and its oxidation and cyclization to the COF-670-hydrazide (b) and COF-670-diazole (c). 6-Fold interpenetration of COF-670-hydrazine (d) and overlay of PXRD patterns of COF-670-hydrazine modeled structures (from 1-fold to 7-fold) and its experimental PXRD pattern (e). PXRD patterns of simulated COF-670-hydrazine compared to the experimental ones of COF-670-hydrazine, COF-670-hydrazide, COF-670-thiadiazole, and COF-670-oxadiazole (f).

We synthesized a series of 2D and 3D diazole-linked COFs by applying a retrosynthetic strategy. This involved first the synthesis of the hydrazine-linked frameworks, followed by oxidation and cyclization to afford the hydrazine, oxadiazole-, and thiadiazole-linked structures, in which the synthesis and transformation from hydrazine to hydrazide and to diazole was proven by the ^{15}N multi-CP-MAS NMR. In addition, we subjected the frameworks to isothermal water sorption analysis. This not only allowed us to discover new structures capable of water harvesting from desert air, but also provided us with additional insight into the micro- and macroscopic changes occurring in the framework. Importantly, we found that even small

modifications of the molecular structures of the frameworks can lead to impactful differences in the water isotherm profiles. Overall, this study expands the scope of COF chemistry to include crystallization of irreversible linkages and shows that these new systems are able to extract water from low-humidity air.

ASSOCIATED CONTENT

Supporting Information

The Supporting Information is available free of charge on the ACS Publications website.

Synthesis and full characterization of COFs including EA, FT-IR spectroscopy, NMR spectra, PXRD data, computational modeling, gas uptake measurements, TGA, and water isotherms (PDF).

X-ray crystallographic data for COF-670-hydrazine (CIF)

AUTHOR INFORMATION

Corresponding Author

*Omar Yaghi: yaghi@berkeley.edu

Author Contributions

H.L.N. and C.G. conceived the idea. H.L.N, C.G., and A.M. synthesized and characterized materials. N.H. and A.L. collected and interpreted data on water vapor sorption and quantitative ^{15}N-NMR spectra, respectively. O.M.Y directed the project. The manuscript was written through contributions of all authors. $^{\Diamond}$H.L.N and C.G. contributed equally.

ABBREVIATIONS

COFs, covalent organic frameworks; EA, elemental analysis; FT-IR, Fourier-transform infrared spectroscopy; NMR, nuclear magnetic resonance spectroscopy; PXRD, powder X-ray diffraction; TGA, thermogravimetric analysis.

REFERENCES

(1) Hawker, C. J.; Wooley, K. L. The Convergence of Synthetic Organic and Polymer Chemistries. *Science* **2005**, *309*, 1200–1205.

(2) Fracaroli, A. M.; Siman, P.; Nagib, D. A.; Suzuki, M.; Furukawa, H.; Toste, F. D.; Yaghi, O. M. Seven Post-Synthetic Covalent Reactions in Tandem Leading to Enzyme-like Complexity within Metal–Organic Framework Crystals. *J. Am. Chem. Soc.* **2016**, *138*, 8352–8355.

(3) Yaghi, O. M. .; Kalmutzki, M. J. .; Diercks, C. S. *Introduction to Reticular Chemistry: Metal-Organic Frameworks and Covalent Organic Frameworks*; Wiley-VCH: Weinheim, 2019.

(4) Kalaj, M.; Cohen, S. M. Postsynthetic Modification: An Enabling Technology for the Advancement of Metal–Organic Frameworks. *ACS Cent. Sci.* **2020**, *6*, 1046–1057.

(5) Waller, P. J.; Lyle, S. J.; Osborn Popp, T. M.; Diercks, C. S.; Reimer, J. A.; Yaghi, O. M. Chemical Conversion of Linkages in Covalent Organic Frameworks. *J. Am. Chem. Soc.* **2016**, *138*, 15519–15522.

(6) Lyle, S. J.; Osborn Popp, T. M.; Waller, P. J.; Pei, X.; Reimer, J. A.; Yaghi, O. M. Multistep Solid-State Organic Synthesis of Carbamate-Linked Covalent Organic Frameworks. *J. Am. Chem. Soc.* **2019**, *141*, 11253–11258.

(7) Lyle, S. J.; Waller, P. J.; Yaghi, O. M. Covalent Organic Frameworks: Organic Chemistry Extended into Two and Three Dimensions. *Trends Chem.* **2019**, *1*, 172–184.

(8) Segura, J. L.; Royuela, S.; Mar Ramos, M. Post-Synthetic Modification of Covalent Organic Frameworks. *Chem. Soc. Rev.* **2019**, *48*, 3903–3945.

(9) Diercks, C. S.; Yaghi, O. M. The Atom, the Molecule, and the Covalent Organic Framework. *Science* **2017**, *355*, eaal1585.

(10) Lohse, M. S.; Bein, T. Covalent Organic Frameworks: Structures, Synthesis, and Applications. *Adv. Funct. Mater.* **2018**, *28*, 1705553.

(11) Geng, K.; He, T.; Liu, R.; Tan, K. T.; Li, Z.; Tao, S.; Gong, Y.; Jiang, Q.; Jiang, D. Covalent Organic Frameworks: Design, Synthesis, and Functions. *Chem. Rev.* **2020**, *120*, 8814–8933.

(12) Haase, F.; Lotsch, B. V. Solving the COF Trilemma: Towards Crystalline, Stable and Functional Covalent Organic Frameworks. *Chem. Soc. Rev.* **2020**, *49*, 8469–8500.

(13) Haase, F.; Troschke, E.; Savasci, G.; Banerjee, T.; Duppel, V.; Dörfler, S.; Grundei, M. M. J.; Burow, A. M.; Ochsenfeld, C.; Kaskel, S.; Lotsch, B. V. Topochemical Conversion of an Imine- into a Thiazole-Linked Covalent Organic Framework Enabling Real Structure Analysis. *Nat. Commun.* **2018**, *9*, 2600.

(14) Waller, P. J.; Alfaraj, Y. S.; Diercks, C. S.; Jarenwattananon, N. N.; Yaghi, O. M. Conversion of Imine to Oxazole and Thiazole Linkages in Covalent Organic Frameworks. *J. Am. Chem. Soc.* **2018**, *140*, 9099–9103.

(15) Cusin, L.; Peng, H.; Ciesielski, A.; Samorì, P. Chemical Conversion and Locking of the Imine Linkage: Enhancing the Functionality of Covalent Organic Frameworks. *Angew. Chem. Int. Ed.* **2021**, *60*, 14236–14250.

(16) Fathieh, F.; Kalmutzki, M. J.; Kapustin, E. A.; Waller, P. J.; Yang, J.; Yaghi, O. M. Practical Water Production from Desert Air. *Sci. Adv.* **2018**, *4*, eaat3198.

(17) Hanikel, N.; Pei, X.; Ccheda, S.; Lyu, H.; Jeong, W.; Sauer, J.; Gagliardi, L.; Yaghi, O. M. Evolution of Water Structures in Metal-Organic Frameworks for Improved Atmospheric Water Harvesting. *Science* **2021**, *in press*.

(18) Massiot, D.; Fayon, F.; Capron, M.; King, I.; Le Calvé, S.; Alonso, B.; Durand, J.-O.; Bujoli, B.; Gan, Z.; Hoatson, G. Modelling One- and Two-Dimensional Solid-State NMR Spectra. *Magn. Reson. Chem.* **2002**, *40*, 70–76.

(19) Sek, D.; Siwy, M.; Bijak, K.; Grucela-Zajac, M.; Malecki, G.; Smolarek, K.; Bujak, L.; Mackowski, S.; Schab-Balcerzak, E. Comparative Studies of Structural, Thermal, Optical, and Electrochemical Properties of Azines with Different End Groups with Their Azomethine Analogues toward Application in (Opto)Electronics. *J. Phys. Chem. A* **2013**, *117*, 10320–10332.

(20) Dimitrowa, K.; Hauschild, J.; Zaschke, H.; Schubert, H. Kristallin-Flüssige 1,3,4-Thiadiazole. I. Biphenyl- Und Terphenylanaloge 1,3,4-Thiadiazole. *J. für Prakt. Chemie* **1980**, *322*, 933–944.

(21) Du, Y.; Wan, Z.; Chen, L.; Wu, L. One Pot Solvent-Free Solid State Synthesis, Photophysical Properties and Crystal Structure of Substituted Azole Derivatives. *J. Mol. Struct.* **2019**, *1193*, 315–325.

(22) Li, Z.; Feng, X.; Zou, Y.; Zhang, Y.; Xia, H.; Liu, X.; Mu, Y. A

2D Azine-Linked Covalent Organic Framework for Gas Storage Applications. *Chem. Commun.* **2014**, *50*, 13825–13828.

(23) Stegbauer, L.; Hahn, M. W.; Jentys, A.; Savasci, G.; Ochsenfeld, C.; Lercher, J. A.; Lotsch, B. V. Tunable Water and CO2 Sorption Properties in Isostructural Azine-Based Covalent Organic Frameworks through Polarity Engineering. *Chem. Mater.* **2015**, *27*, 7874–7881.

(24) Dalapati, S.; Jin, S.; Gao, J.; Xu, Y.; Nagai, A.; Jiang, D. An Azine-Linked Covalent Organic Framework. *J. Am. Chem. Soc.* **2013**, *135*, 17310–17313.

(25) Furukawa, H.; Gándara, F.; Zhang, Y. B.; Jiang, J.; Queen, W. L.; Hudson, M. R.; Yaghi, O. M. Water Adsorption in Porous Metal-Organic Frameworks and Related Materials. *J. Am. Chem. Soc.* **2014**, *136*, 4369–4381.

(26) Nguyen, H. L.; Hanikel, N.; Lyle, S. J.; Zhu, C.; Proserpio, D. M.; Yaghi, O. M. A Porous Covalent Organic Framework with Voided Square Grid Topology for Atmospheric Water Harvesting. *J. Am. Chem. Soc.* **2020**, *142*, 2218–2221.

(27) Karak, S.; Kandambeth, S.; Biswal, B. P.; Sasmal, H. S.; Kumar, S.; Pachfule, P.; Banerjee, R. Constructing Ultraporous Covalent Organic Frameworks in Seconds via an Organic Terracotta Process. *J. Am. Chem. Soc.* **2017**, *139*, 1856–1862.

(28) Biswal, B. P.; Kandambeth, S.; Chandra, S.; Shinde, D. B.; Bera, S.; Karak, S.; Garai, B.; Kharul, U. K.; Banerjee, R. Pore Surface Engineering in Porous, Chemically Stable Covalent Organic Frameworks for Water Adsorption. *J. Mater. Chem. A* **2015**, *3*, 23664–23669.

Table of Content